



Phase stability and transport characteristics of $(\text{ZrO}_2)_{1-x}(\text{Sc}_2\text{O}_3)_x(\text{CeO}_2)_y$ and $(\text{ZrO}_2)_{1-x-y-z}(\text{Sc}_2\text{O}_3)_x(\text{CeO}_2)_y(\text{Y}_2\text{O}_3)_z$ solid solution crystals



D.A. Agarkov^{a, b}, M.A. Borik^c, V.T. Bublik^d, A.S. Chislov^{c, d}, A.V. Kulebyakin^c, I.E. Kuritsyna^a, V.A. Kolotygin^a, E.E. Lomonova^c, F.O. Milovich^{d, *}, V.A. Myzina^c, V.V. Osiko^c, N. Yu. Tabachkova^{c, d}

^a Institute of Solid State Physics, Russian Academy of Sciences, Academician Osip'yan Str. 2, 142432, Chernogolovka, Moscow District, Russia

^b Moscow Institute of Physics and Technology, Institutsky Lane 9, 141700, Dolgoprudny, Moscow District, Russia

^c Prokhorov General Physics Institute, Russian Academy of Sciences, Vavilov Str. 38, 119991, Moscow, Russia

^d National University of Science and Technology (MISIS), Leninskiy Prospekt 4, 119049, Moscow, Russia

ARTICLE INFO

Article history:

Received 21 September 2018

Received in revised form

14 March 2019

Accepted 18 March 2019

Available online 21 March 2019

Keywords:

Single crystals

Solid oxide fuel cell

Solid solutions

Ionic conducting materials

ZrO₂-Sc₂O₃-CeO₂-Y₂O₃

ABSTRACT

Phase stability and transport characteristics of $(\text{ZrO}_2)_{1-x}(\text{Sc}_2\text{O}_3)_x(\text{CeO}_2)_y$ ($x = 0.08–0.10$; $y = 0.005–0.015$) and $(\text{ZrO}_2)_{1-x-y-z}(\text{Sc}_2\text{O}_3)_x(\text{CeO}_2)_y(\text{Y}_2\text{O}_3)_z$ ($x = 0.08–0.10$; $y = 0.005–0.010$; $z = 0.005–0.020$) melt-grown crystals have been studied after air heat treatment at 1000 °C for 400 h.

Annealing of the $(\text{ZrO}_2)_{1-x}(\text{Sc}_2\text{O}_3)_x(\text{CeO}_2)_y$ crystals caused the formation of a rhombohedral phase and reduced the electrical conductivity of the specimens in the entire test temperature range. Yttrium co-doping of the $(\text{ZrO}_2)_{1-x}(\text{Sc}_2\text{O}_3)_x(\text{CeO}_2)_y$ crystals stabilized the cubic phase for some compositions. In two-phase $(\text{ZrO}_2)_{1-x-y-z}(\text{Sc}_2\text{O}_3)_x(\text{CeO}_2)_y(\text{Y}_2\text{O}_3)_z$ crystals containing a cubic and a tetragonal phases exhibited conductivity degradation. Annealing of cubic crystals caused the formation of the t' phase and increased their conductivity.

© 2019 Elsevier B.V. All rights reserved.

1. Introduction

Scandia stabilized zirconia has the highest electrical conductivity among all the zirconia base solid solutions and is considered to be a promising solid electrolyte for solid oxide fuel cells designed for operation at moderate temperatures (700–900 °C) [1,2]. A significant disadvantage of this material is its tendency to form a rhombohedral phase at a Sc₂O₃ content of 10–12 mol.% and a cubic-rhombohedral phase transition at approx. 600 °C [3,4]. This transition is accompanied with a slight change in the volume of the solid electrolyte which produces stresses capable of destroying the electrolytic cell. Common practice is to stabilize the cubic phase by introducing Y₂O₃ [5–7], Yb₂O₃ [8–10], Gd₂O₃ [11], Sm₂O₃ [11] and CeO₂ [12–14] oxides in the electrolyte. Ceramic materials containing 10 mol.% Sc₂O₃ and 1 mol.% CeO₂ (10Sc1CeSZ) exhibited a

stabilization of the cubic phase up to room temperature and high oxygen/ionic conductivity. In our previous work we studied the phase composition and transport characteristics of $(\text{ZrO}_2)_{1-x-y}(\text{Sc}_2\text{O}_3)_x(\text{CeO}_2)_y$ ($x = 0.08–0.10$; $y = 0.005–0.015$) solid solution crystals grown by directional melt crystallization [15]. We showed that CeO₂ introduction in the $(\text{ZrO}_2)_{1-x}(\text{Sc}_2\text{O}_3)_x$ crystals increases their high-temperature conductivity. The highest conductivity was observed at a CeO₂ content of 0.5 mol.% and a Sc₂O₃ concentration of 8.5–10 mol.%. The phase composition of the crystals depended on the overall concentration of the stabilizing oxides, and a rhombohedral phase existed in the crystals at an overall concentration of the stabilizing oxides of above 10 mol.%. Furthermore, we could not obtain single-phase cubic crystals in the studied composition range. However, we showed that additional yttria doping of the $(\text{ZrO}_2)_{1-x}(\text{Sc}_2\text{O}_3)_x$ crystals stabilized the cubic phase for some of the compositions. Therefore in this work we studied the effect of additional yttria doping of the $(\text{ZrO}_2)_{1-x}(\text{Sc}_2\text{O}_3)_x(\text{CeO}_2)_y$ crystals on the phase composition and transport characteristics of these crystals.

* Corresponding author.

E-mail address: philippmilovich@gmail.com (F.O. Milovich).

Stability of the operation and resource capabilities of SOFC depends on many different factors: the processes of degradation of SOFC materials, processes at the electrode-electrolyte and electrode-interconnect interfaces, the electrochemical activity of the electrodes when interacting with the gaseous environment, etc. Saving high electrical conductivity of solid electrolytes during long-term operation at high temperatures (high-temperature degradation) is one of the key factors determining the efficiency of the SOFC. As a rule, studies of the degradation of solid electrolytes are carried out by means of long-term annealing of the electrolyte at temperatures close to the operating temperature of SOFC [12,17,18]. Conductivity degradation in ceramic solid electrolytes may be associated with processes such as: phase transformations, complex formation between oxygen vacancies and stabilizer's cations, formation of long-range ordered phases, increase of the grain

boundary resistance, increasing impurity segregation at grain boundaries [19–21]. The factors associated with the grain structure of ceramic materials are absent in single crystals. The conductivity of crystals, even in the presence of a twin structure, is determined only by their bulk conductivity [22].

One of the main factors affecting on the conductivity degradation of single crystals is their phase stability during high-temperature annealing.

In this work we studied the phase stability and transport characteristics of melt-grown $(\text{ZrO}_2)_{1-x}(\text{Sc}_2\text{O}_3)_x(\text{CeO}_2)_y$ ($x = 0.08\text{--}0.10$; $y = 0.005\text{--}0.015$) and $(\text{ZrO}_2)_{1-x-y-z}(\text{Sc}_2\text{O}_3)_x(\text{CeO}_2)_y(\text{Y}_2\text{O}_3)_z$ ($x = 0.08\text{--}0.10$; $y = 0.005\text{--}0.010$; $z = 0.005\text{--}0.020$) crystals after air heat treatment at 1000 °C for 400 h.

2. Experimental

$(\text{ZrO}_2)_{1-x}(\text{Sc}_2\text{O}_3)_x(\text{CeO}_2)_y$ ($x = 0.08\text{--}0.10$; $y = 0.005\text{--}0.015$) and $(\text{ZrO}_2)_{1-x-y-z}(\text{Sc}_2\text{O}_3)_x(\text{CeO}_2)_y(\text{Y}_2\text{O}_3)_z$ ($x = 0.08\text{--}0.10$; $y = 0.005\text{--}0.010$; $z = 0.005\text{--}0.020$) solid solution crystals were grown by directional melt crystallization in a cold crucible [23].

The crystals were then annealed in a Supertherm HT04/16 high-temperature resistance furnace in air at 1000 °C for 400 h. This temperature was chosen due to its proximity to the operation temperatures of solid oxide fuel cells. For moderate temperature solid oxide fuel cells (700–900 °C), the stability of these materials must be higher due to the lower diffusion rate. The exposure time of 400 h was chosen because, according to the preliminary data of life tests, significant conductivity degradation occurs at the operation temperature in the first 200–400 h.

Phase analysis was carried out by X-ray diffraction on a Bruker D8 diffractometer in $\text{CuK}\alpha$ radiation and using Raman scattering. The excitation source was a 532 nm laser.

The density of the crystals was measured by hydrostatic weighing on a Sartorius hydrostatic weighing instrument. The microstructure of the crystals was examined by optical microscopy under a Discovery V12 stereoscopic microscope.

The conductivity of the zirconia base crystals was measured in the 400–900 °C range using a Solartron SI 1260 frequency analyzer in the 1 Hz–5 MHz range. The measurements were carried out on crystal plates size of $7 \times 7 \text{ mm}^2$ and thickness of 0.5 mm with symmetrically connected Pt electrodes. Platinum electrodes were annealed in air at the temperature 950 °C for 1 h. The specific conductivity of the crystals was calculated based on the data retrieved from the impedance spectra taking into account the specimen dimensions.

Table 1
Compositions, brief notations and densities of as-grown and as-annealed crystals.

| Composition | Notation | Density, g/cm ³ | |
|--|--------------|----------------------------|-------------------|
| | | As-Grown [15] | As-Annealed |
| $(\text{ZrO}_2)_{0.90}(\text{Sc}_2\text{O}_3)_{0.085}(\text{CeO}_2)_{0.015}$ | 8.5Sc1.5CeSZ | 5.787 ± 0.001 | 5.783 ± 0.001 |
| $(\text{ZrO}_2)_{0.90}(\text{Sc}_2\text{O}_3)_{0.09}(\text{CeO}_2)_{0.01}$ | 9Sc1CeSZ | 5.791 ± 0.001 | 5.789 ± 0.001 |
| $(\text{ZrO}_2)_{0.90}(\text{Sc}_2\text{O}_3)_{0.095}(\text{CeO}_2)_{0.005}$ | 9.5Sc0.5CeSZ | 5.778 ± 0.001 | 5.759 ± 0.001 |

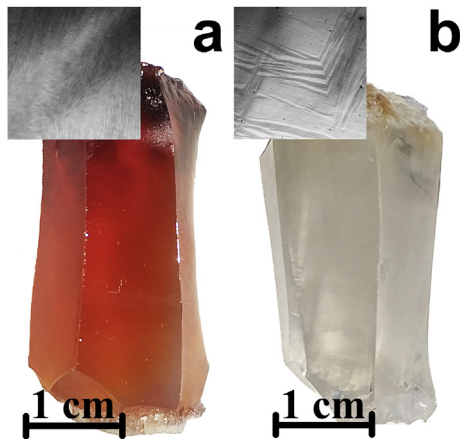


Fig. 1. Appearance of (a) as-grown and (b) As-annealed 8.5Sc1.5CeSZ crystal. Insets show optical microscopic images of crystal microstructure.

Table 2
Phase Composition and Lattice Parameters of ScCeSZ Crystals As-Grown and As-Annealed in Air at 1000 °C for 400 h.

| | As-Grown | | | | As-Annealed | | | |
|--------------|----------|--------------------|--------------------|-----------|-------------|--------------------|--------------------|-----------|
| | Phase | Weight Fraction, % | Lattice Parameters | | Phase | Weight Fraction, % | Lattice Parameters | |
| | | | a, nm | c, nm | | | a, nm | c, nm |
| 8.5Sc1.5CeSZ | t | 80(2) | 0.3597(1) | 0.5112(1) | t | 80(2) | 0.3598(1) | 0.5115(1) |
| | c | 20(2) | 0.5092(1) | | c | 10(2) | 0.5093(1) | 0.9005(2) |
| 9Sc1CeSZ | t | 85(2) | 0.3597(1) | 0.5110(1) | r | 10(2) | 0.3559(2) | |
| | c | 15(2) | 0.5092(1) | | t | 85(2) | 0.3598(1) | 0.5117(1) |
| | | | | | c | 10(2) | 0.5093(1) | 0.9006(2) |
| 9.5Sc0.5CeSZ | | | | | r | 5(2) | 0.3560(2) | |
| | t | 80(2) | 0.3597(1) | 0.5109(1) | t | 80(2) | 0.3597(1) | 0.5116(1) |
| | c | 20(2) | 0.5092(1) | | c | 5(2) | 0.5093(1) | 0.9005(2) |
| | | | | | r | 15(2) | 0.3559(2) | |

c: cubic modification of ZrO_2 .

t: tetragonal modification of ZrO_2 .

r: rhombohedral modification of ZrO_2 .

3. Results and discussion

3.1. Study of structure and transport characteristics of as-grown and as-annealed $(\text{ZrO}_2)_{1-x}(\text{Sc}_2\text{O}_3)_x(\text{CeO}_2)_y$ crystals

Table 1 summarizes the compositions, brief notations and densities of the as-grown and as-annealed $(\text{ZrO}_2)_{1-x}(\text{Sc}_2\text{O}_3)_x(\text{CeO}_2)_y$ crystals. We studied the effect of heat treatment on the phase stability and transport characteristics of crystals with an overall stabilizing oxide concentration of 10 mol.% because it was shown earlier [15] that a rhombohedral phase forms in the crystals if this concentration is exceeded.

Fig. 1 shows the appearance of the as-grown and as-annealed 8.5Sc1.5CeSZ crystal. It can be seen that the as-annealed crystal is colorless. This effect is due to the oxidation of the Ce^{3+} ions to Ce^{4+} . The crystal microstructure presented in the insets clearly suggests the formation of large inclusions which are typical of a rhombohedral phase [24]. Similar changes occurred in the 9Sc1CeSZ and 9.5Sc0.5CeSZ crystals.

The phase composition of the crystals as-grown and as-annealed at 1000 °C for 400 h was studied by X-ray diffraction. The results are summarized in Table 2.

As can be seen from Table 2, the phase composition of the as-grown crystals was a mixture of the tetragonal and the cubic phases. Annealing changed the phase composition of the crystals by causing the formation of a rhombohedral phase. The concentration of the rhombohedral phase increases due to a decrease in the concentration of the cubic phase, whereas the content of the tetragonal phase changes but slightly. In the as-annealed state the lattice parameter a of the tetragonal phase changes little if any, whereas the parameter c increases, indicating a shift of the oxygen atoms along the c axis. No significant changes in the lattice parameters of the cubic phase were observed. The observed change in the phase composition of the specimens agrees with the density data presented in Table 1. The lower density of the as-annealed specimens is caused by the formation of the rhombohedral phase which has a lower density compared with the cubic and the tetragonal phases.

Fig. 2 shows the specific conductivity of the as-grown and as-annealed test ScCeSZ crystals in Arrhenius coordinates. The temperature functions of the specific volume conductivity of all the as-annealed test crystals exhibit clear conductivity breakdowns in the 600–800 °C range testifying to the presence of a rhombohedral phase in the specimens. It can also be seen that annealing reduces the conductivity of the specimens in the entire test temperature range. Our estimates show that the conductivity drops after annealing by 10–20% for 1173 K.

Thus, we have found that long-term high-temperature annealing of ScCeSZ crystals with an overall stabilizing oxide concentration of 10 mol.% leads to the appearance of the rhombohedral phase and causes conductivity degradation.

3.2. Study of structure and transport characteristics of as-grown and as-annealed $(\text{ZrO}_2)_{1-x-y-z}(\text{Sc}_2\text{O}_3)_x(\text{CeO}_2)_y(\text{Y}_2\text{O}_3)_z$ crystals

The data presented in the previous section show that the introduction of ceria in $(\text{ZrO}_2)_{1-x}(\text{Sc}_2\text{O}_3)_x$ crystals in the studied concentration range did not produce single-phase cubic crystals. It has been reported, however, that additional yttria doping of $(\text{ZrO}_2)_{1-x}(\text{Sc}_2\text{O}_3)_x$ crystals stabilized the cubic phase for some compositions in ceramic and crystalline specimens [5–7,16]. We therefore synthesized a range of $(\text{ZrO}_2)_{1-x}(\text{Sc}_2\text{O}_3)_x(\text{CeO}_2)_y$ solid solutions co-doped with Y_2O_3 . The compositions were chosen taking into account earlier data [15] which showed that the maximum conductivity occurs in $(\text{ZrO}_2)_{1-x}(\text{Sc}_2\text{O}_3)_x(\text{CeO}_2)_y$ crystals

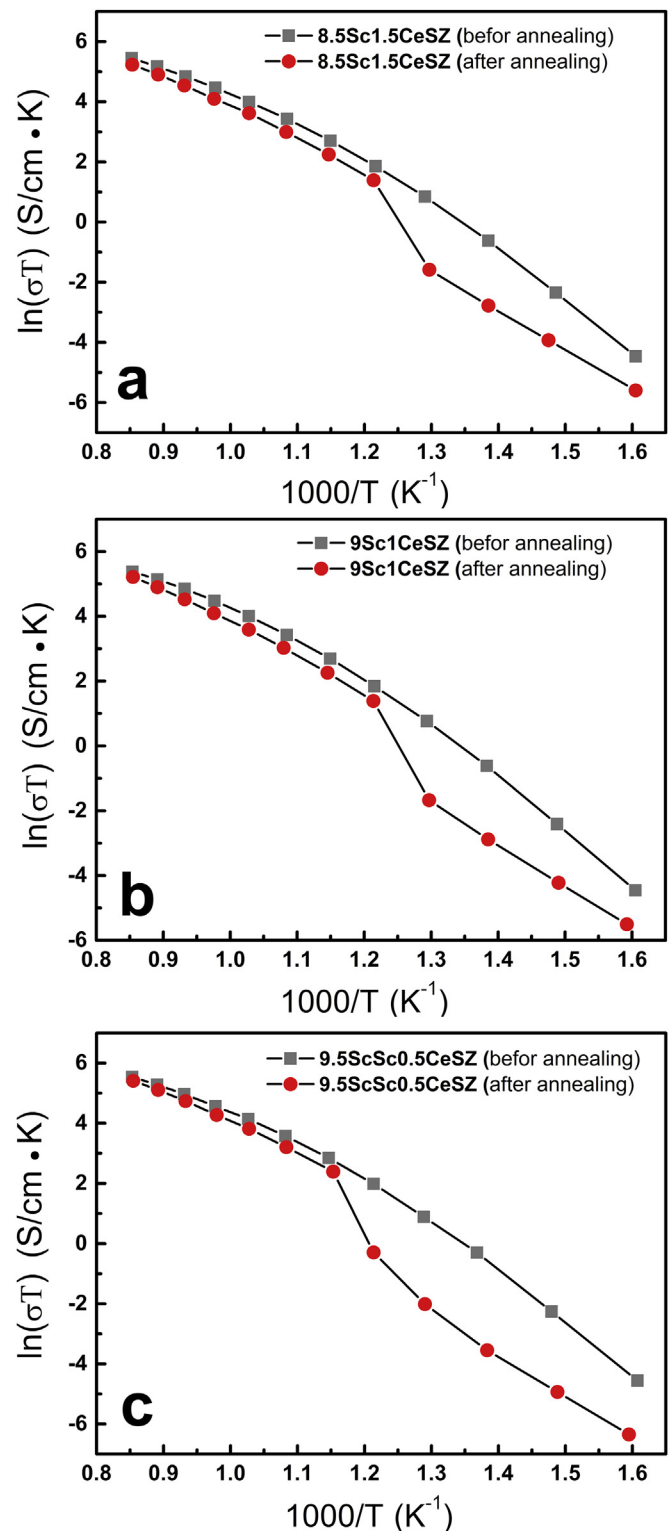


Fig. 2. Specific bulk conductivity of as-grown and as-annealed (a) 8.5Sc1.5CeSZ, (b) 9Sc1CeSZ and (c) 9.5Sc0.5CeSZ crystals as a function of temperature.

containing 0.5 mol.% CeO_2 .

Table 3 summarizes the compositions, brief notations and densities of the as-grown and as-annealed $(\text{ZrO}_2)_{1-x-y-z}(\text{Sc}_2\text{O}_3)_x(\text{CeO}_2)_y(\text{Y}_2\text{O}_3)_z$ crystals.

Fig. 3 shows the appearance of as-grown ScCeYSZ crystals. The 8Sc0.5Ce1.5YSZ crystals (Fig. 3a) were opaque which indirectly

Table 3
Compositions, brief notations and densities of as-grown and as-annealed crystals.

| Composition | Notation | Density, g/cm ³ | |
|--|------------------|----------------------------|---------------|
| | | As-Grown | As-Annealed |
| (ZrO ₂) _{0.91} (Sc ₂ O ₃) _{0.08} (CeO ₂) _{0.005} (Y ₂ O ₃) _{0.005} | 8Sc0.5Ce0.5YSZ | 5.829 ± 0.001 | 5.799 ± 0.001 |
| (ZrO ₂) _{0.90} (Sc ₂ O ₃) _{0.08} (CeO ₂) _{0.005} (Y ₂ O ₃) _{0.015} | 8Sc0.5Ce1.5YSZ | 5.841 ± 0.004 | 5.775 ± 0.001 |
| (ZrO ₂) _{0.895} (Sc ₂ O ₃) _{0.08} (CeO ₂) _{0.005} (Y ₂ O ₃) _{0.02} | 8Sc0.5Ce2YSZ | 5.829 ± 0.001 | 5.807 ± 0.001 |
| (ZrO ₂) _{0.90} (Sc ₂ O ₃) _{0.09} (CeO ₂) _{0.005} (Y ₂ O ₃) _{0.005} | 9Sc0.5Ce0.5YSZ | 5.785 ± 0.002 | 5.756 ± 0.001 |
| (ZrO ₂) _{0.885} (Sc ₂ O ₃) _{0.009} (CeO ₂) _{0.005} (Y ₂ O ₃) _{0.02} | 9Sc0.5Ce2YSZ | 5.755 ± 0.003 | 5.759 ± 0.001 |
| (ZrO ₂) _{0.895} (Sc ₂ O ₃) _{0.095} (CeO ₂) _{0.005} (Y ₂ O ₃) _{0.005} | 9.5Sc0.5Ce0.5YSZ | 5.767 ± 0.001 | 5.756 ± 0.001 |
| (ZrO ₂) _{0.89} (Sc ₂ O ₃) _{0.1} (CeO ₂) _{0.005} (Y ₂ O ₃) _{0.005} | 10Sc0.5Ce0.5YSZ | 5.755 ± 0.001 | 5.720 ± 0.001 |

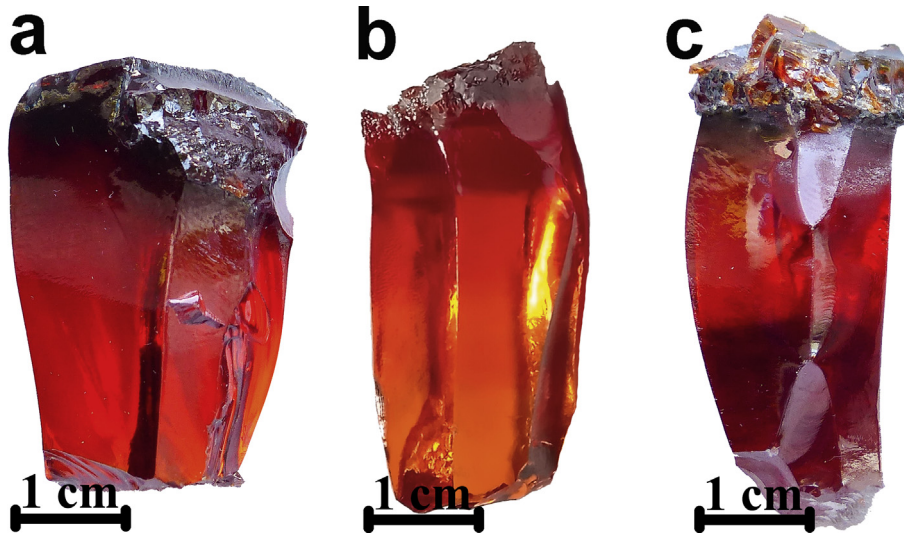


Fig. 3. Appearance of as-grown (a) 8Sc0.5Ce1.5YSZ, (b) 8Sc0.5Ce2YSZ and (c) 10Sc0.5Ce0.5YSZ crystals.

suggests the presence of a second phase. The 8Sc0.5Ce1.5YSZ, 9Sc0.5Ce0.5YSZ and 9.5Sc0.5Ce0.5YSZ crystals had a similar appearance. The 8Sc0.5Ce2YSZ (Fig. 3b) and 9Sc0.5Ce2YSZ crystals were transparent. The 10Sc0.5Ce0.5YSZ crystals were inhomogeneous, with opaque bottom parts and transparent top parts (Fig. 3c). Annealing of the ScCeYSZ crystals made them colorless, by analogy with the ScCeSZ ones. No notable changes in their microstructure were observed.

Table 4 summarizes X-ray diffraction data for the as-grown and as-annealed ScCeYSZ crystals.

Yttria co-doping of the as-grown crystals caused the following

Table 4
Phase Composition and Lattice Parameters of ScCeYSZ Crystals As-Grown and As-Annealed in Air at 1000 °C for 400 h.

| Sample | Phase | Before annealing | | After annealing | |
|------------------|-------|--------------------|-----------|--------------------|-----------|
| | | Lattice parameters | | Lattice parameters | |
| | | a, nm | c, nm | a, nm | c, nm |
| 8Sc0.5Ce0.5YSZ | t | 0.3599(1) | 0.5115(1) | 0.3598(1) | 0.5125(1) |
| | c | 0.5094(1) | | 0.5094(1) | |
| 8Sc0.5Ce1.5YSZ | t | 0.3604(1) | 0.5114(1) | 0.3604(1) | 0.5115(1) |
| | c | 0.5098(1) | | 0.5098(1) | |
| 8Sc0.5Ce2YSZ | c | 0.5102(1) | | 0.5101(1) | |
| 9Sc0.5Ce0.5YSZ | t | 0.3600(1) | 0.5106(1) | 0.3601(1) | 0.5107(1) |
| | c | 0.5093(1) | | 0.5092(1) | |
| 9Sc0.5Ce2YSZ | c | 0.5101(1) | | 0.5101(1) | |
| 9.5Sc0.5Ce0.5YSZ | t | 0.3600(1) | 0.5107(1) | 0.3601(1) | 0.5107(1) |
| | c | 0.5093(1) | | 0.5093(1) | |
| 10Sc0.5Ce0.5YSZ | r | 0.3560(2) | 0.9007(2) | 0.3560(2) | 0.9007(2) |
| | c | 0.5092(1) | | 0.5093(1) | |

changes. Addition of 0.5 mol.% Y₂O₃ to any of the synthesized crystals did not produce single-phase cubic crystals. In the crystals containing 8 mol.% Sc₂O₃ stabilization of the cubic phase is observed only with additional doping with 2 mol.% Y₂O₃. Increase of Y₂O₃ content in the crystals of this series (8Sc0.5CexYSZ) leads a monotonous increase of the lattice parameter of the cubic phase.

Fig. 4 shows TEM images of crystals of different phase composition. The regions of the tetragonal phase contained twins in two-phase (c + t) crystals. As an example, Fig. 4 (a) shows an image of twins of the tetragonal phase in an 8Sc0.5Ce0.5YSZ crystal. Fig. 4 (b) shows an image characteristic of the structure of a cubic crystal. Large twins inherent of the rhombohedral phase are observed in a 10Sc0.5Ce0.5YSZ crystal (Fig. 4 (c)).

Annealing of the crystals did not cause any fundamental changes in their phase composition. Except for the 8Sc0.5Ce0.5YSZ crystal, the lattice parameters of the crystalline structure remained almost the same after annealing in all the other crystals.

In the 8Sc0.5Ce0.5YSZ specimen which had an overall stabilizing oxide concentration of 9 mol.%, annealing increased the lattice parameter *c* of the tetragonal phase and reduced the lattice parameter *a*. The increase in the tetragonality observed after annealing can be accounted for by a decrease in the size of the cerium ions as a result of the Ce³⁺ → Ce⁴⁺ transition and a decrease in the number of vacancies caused by the fact that the replacement of the Zr⁴⁺ ion in the lattice for Ce⁴⁺ one in the lattice does not require charge compensation. In all the other crystals with a higher overall concentration of stabilizing oxides the lattice parameters remained almost the same after annealing.

We also studied the phase composition of the crystals using

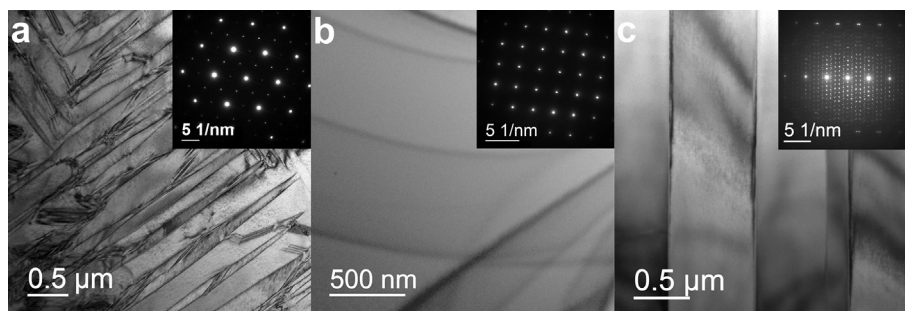


Fig. 4. TEM images of the tetragonal phase twins in the 8Sc0.5Ce0.5YSZ crystal (a), of the 8Sc0.5Ce2YSZ cubic crystal (b), and twins of a rhombohedral phase in a 10Sc0.5Ce0.5YSZ crystal (c). The insets show electron diffraction patterns of the corresponding crystal regions.

Raman scattering. Fig. 5 shows the Raman spectra of some ScCeYSZ specimens.

Comparison of the Raman spectra of the as-grown and as-annealed crystals shows that the spectrum of the as-annealed 9Sc0.5Ce0.5YSZ crystal becomes closer to the tetragonal phase spectrum. Similar changes were observed in two-phase crystals containing the cubic and the tetragonal phases (8Sc0.5Ce0.5YSZ, 8Sc0.5Ce1.5YSZ and 9.5Sc0.5Ce0.5YSZ). The Raman spectra of the as-grown 9Sc0.5Ce2YSZ and 8Sc0.5Ce2YSZ crystals exhibit peaks typical of cubic crystals. The Raman spectra of the as-annealed 9Sc0.5Ce2YSZ and 8Sc0.5Ce2YSZ crystals contain an additional peak in the vicinity of 470 cm^{-1} which is attributed to the t'' phase [25]. The tetragonality of this phase is 1, but its space group is $P4_2/nmc$ due to a shift of the oxygen ions in the anion sublattice [26]. Noteworthy, the as-annealed 8Sc0.5Ce2YSZ and 9Sc0.5Ce2YSZ crystals remain homogeneous and transparent. The Raman spectra of the bottom part of the 10Sc0.5Ce0.5YSZ crystals, whether as-grown or as-annealed, are typical of crystals containing the rhombohedral phase, but in the as-annealed crystals the spectral lines become narrower and more explicit. The Raman spectra of the top part of the as-grown 10Sc0.5Ce0.5YSZ crystal exhibit peaks typical of cubic crystals. In the as-annealed crystals the Raman

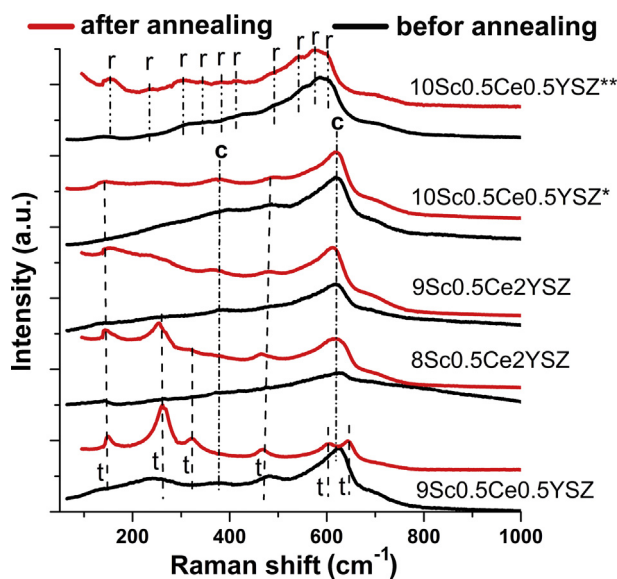


Fig. 5. Raman Spectra of ScCeYSZ Crystals As-Grown and As-Annealed in Air at $1000\text{ }^\circ\text{C}$ for 400 h (*top of the crystal,** bottom of the crystal).

spectra of the top part of the 10Sc0.5Ce0.5YSZ crystal exhibit an additional peak in the vicinity of 470 cm^{-1} corresponding to the t'' phase, by analogy with the single-phase cubic 9Sc0.5Ce2YSZ and 8Sc0.5Ce2YSZ crystals.

Noteworthy, Raman spectroscopy allows identifying minor changes in local structures resulting from long-term annealing.

Fig. 6 shows the specific conductivity of the as-grown test ScCeYSZ crystals in Arrhenius coordinates. These data show that the breakdown in the conductivity curve that is typical of the rhombohedral phase is only observed in the curves for the bottom part of the 10Sc0.5Ce0.5YSZ crystal, which is in agreement with the phase composition data. The high-temperature conductivity is almost the same for different parts of the 10Sc0.5Ce0.5YSZ crystal.

Fig. 7 shows the conductivity of the $(\text{ZrO}_2)_{0.99-x}(\text{Sc}_2\text{O}_3)_x(\text{CeO}_2)_{0.005}(\text{Y}_2\text{O}_3)_{0.005}$ crystals as a function of Sc_2O_3 content for different temperatures. The conductivity of the crystals increases with Sc_2O_3 concentration and has a weak maximum at a Sc_2O_3 content of 9.5 mol.%. Comparison of these data with earlier results for $(\text{ZrO}_2)_{1-x}(\text{Sc}_2\text{O}_3)_x(\text{CeO}_2)_{0.005}$ crystals [15] shows that even the introduction of as little as 0.5 mol.% Y_2O_3 reduces the conductivity of the crystals. The conductivities of single-phase cubic 8Sc0.5Ce2YSZ and 9Sc0.5Ce2YSZ crystals at 1173 K were 0.144 and 0.154 S/cm, respectively.

The conductivity of the as-annealed crystals changed in

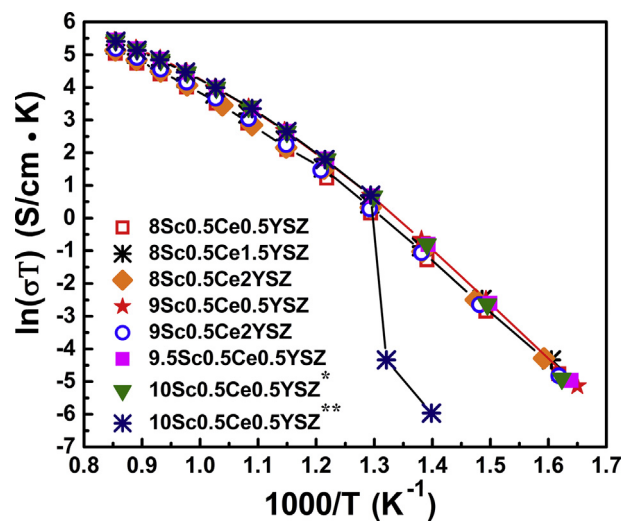


Fig. 6. Specific Bulk Conductivity of As-Grown ScCeYSZ Crystals as a Function of Temperature. (*top of the crystal,** bottom of the crystal).

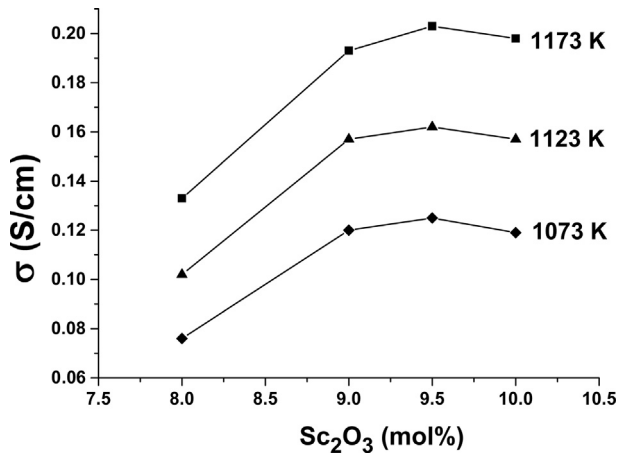


Fig. 7. Conductivity of $(\text{ZrO}_2)_{0.99-x}(\text{Sc}_2\text{O}_3)_x(\text{CeO}_2)_{0.005}(\text{Y}_2\text{O}_3)_{0.005}$ crystals as a function of Sc_2O_3 content for different temperatures.

different manners (Fig. 8) for the inhomogeneous 10Sc0.5Ce0.5YSZ crystal. We only measured its conductivity for specimens cut out of the top part of the crystal.

In the two-phase crystals (8Sc0.5Ce0.5YSZ, 9Sc0.5Ce0.5YSZ, 9.5Sc0.5Ce0.5YSZ and 8Sc0.5Ce1.5YSZ) containing the cubic and the tetragonal phases, the conductivity degraded, with the degradation being the smallest (7%) for the 8Sc0.5Ce1.5YSZ with the highest Y_2O_3 content. However, the maximum conductivity of the as-annealed crystals of this series was observed for the 9.5Sc0.5Ce0.5YSZ composition.

The conductivity of the single-phase as-annealed cubic 8Sc0.5Ce2YSZ and 9Sc0.5Ce2YSZ crystals increased by 20 and 30%, respectively. The conductivity also increased in the specimens cut out of the top part of the 10Sc0.5Ce0.5YSZ crystal which had a cubic structure in the as-grown state. A slight increase in the conductivity was also observed earlier [27] in as-annealed at 1000 °C ceramic 12ScSZ and 2Yb10ScSZ specimens but they had a rhombohedral phase unlike the crystals studied here. This behavior of conductivity can be attributed to the formation of the t'' phase during annealing of the crystals, as supported by the Raman data. As shown earlier [16], ZrO_2 - Y_2O_3 solid solution crystals containing the t'' phase had the highest conductivity. This effect can be

alternatively accounted for by the insufficiently long annealing forming a thermodynamically metastable structure which may transform to a more stable tetragonal phase during further annealing. More detailed study of this effect will require more thorough conductivity measurements after longer annealing.

4. Conclusion

$(\text{ZrO}_2)_{1-x}(\text{Sc}_2\text{O}_3)_x(\text{CeO}_2)_y$ ($x = 0.08$ – 0.10 ; $y = 0.005$ – 0.015) and $(\text{ZrO}_2)_{1-x-y-z}(\text{Sc}_2\text{O}_3)_x(\text{CeO}_2)_y(\text{Y}_2\text{O}_3)_z$ ($x = 0.08$ – 0.10 ; $y = 0.005$ – 0.010 ; $z = 0.005$ – 0.020) solid solution crystals were grown by directional crystallization in a cold crucible.

X-ray diffraction and Raman studies of the phase composition of the crystals have shown that a rhombohedral phase in as-annealed $(\text{ZrO}_2)_{1-x}(\text{Sc}_2\text{O}_3)_x(\text{CeO}_2)_y$ crystals forms due to a decrease in the concentration of the cubic phase, whereas the content of the tetragonal phase changes but slightly. Annealing reduces the conductivity of the specimens over the entire test temperature range. Our estimates show that the conductivity drops by 10–20% as a result of annealing at 1173 K.

Yttria co-doping of the $(\text{ZrO}_2)_{1-x}(\text{Sc}_2\text{O}_3)_x(\text{CeO}_2)_y$ crystals leads to stabilization of the cubic phase only when the content of Y_2O_3 not less than 2 mol.%. Annealing of single-phase cubic 8Sc0.5Ce2YSZ and 9Sc0.5Ce2YSZ crystals caused the formation of the t'' phase as shown by the Raman data. The conductivity of the $(\text{ZrO}_2)_{0.99-x}(\text{Sc}_2\text{O}_3)_x(\text{CeO}_2)_{0.005}(\text{Y}_2\text{O}_3)_{0.005}$ crystals increases with Sc_2O_3 concentration and has a weak maximum at a Sc_2O_3 content of 9.5 mol.%.

Conductivity degradation was observed in two-phase $(\text{ZrO}_2)_{1-x-y-z}(\text{Sc}_2\text{O}_3)_x(\text{CeO}_2)_y(\text{Y}_2\text{O}_3)_z$ crystals containing the cubic and the tetragonal phases. The conductivity of as-annealed single-phase cubic 8Sc0.5Ce2YSZ and 9Sc0.5Ce2YSZ crystals increased by 20 and 30%, respectively. This behavior can be accounted for by the formation of the t'' phase during annealing.

The $(\text{ZrO}_2)_{1-x-y-z}(\text{Sc}_2\text{O}_3)_x(\text{CeO}_2)_y(\text{Y}_2\text{O}_3)_z$ crystals, which have a cubic structure and do not show a tendency to degradation of conductivity, seem to be the most promising for use as solid electrolytes for SOFC. However, the obtained results do not allow us to uniquely identify the most promising compositions, since it is necessary to further study the nature of the change in conductivity during longer annealing.

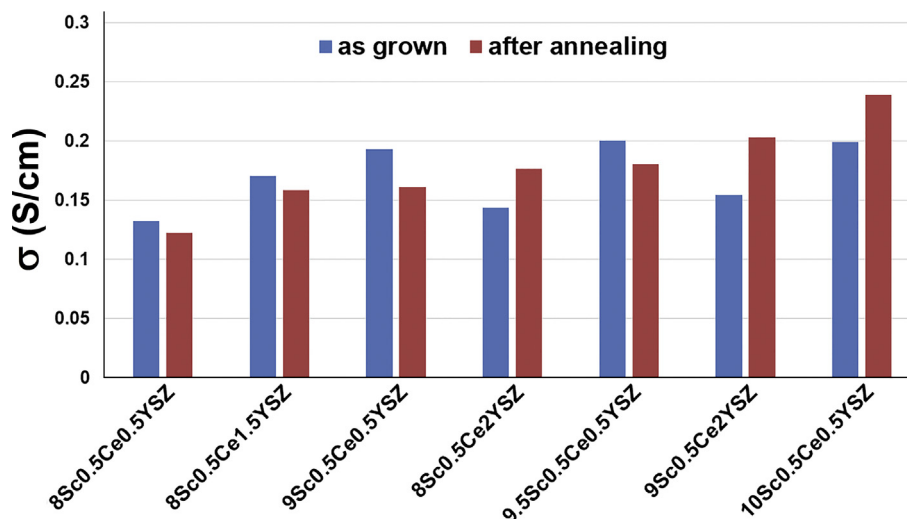


Fig. 8. Conductivity of ScCeYSZ Crystals As-Grown and As-Annealed at 1000 °C for 400 h.

Acknowledgements

The work was carried out with financial support in part from the RSF (grant number 16-13-00056).

References

- [1] S.P.S. Badwal, Materials for solid oxide fuel cells, *Mater. Forum* 21 (1997) 187–224. <https://doi.org/10.1533/9781845694838.280>.
- [2] S.P.S. Badwal, F.T. Ciacchi, D. Milosevic, Scandia–zirconia electrolytes for intermediate temperature solid oxide fuel cell operation, *Solid State Ionics* 136–137 (2000) 91–99. [https://doi.org/10.1016/S0167-2738\(00\)00356-8](https://doi.org/10.1016/S0167-2738(00)00356-8).
- [3] O. Yamamoto, Y. Arati, Y. Takeda, N. Imanishi, Y. Mizutani, M. Kawai, Y. Nakamura, Electrical conductivity of stabilized zirconia with ytterbia and scandia, *Solid State Ionics* 79 (1995) 137–142. [https://doi.org/10.1016/0167-2738\(95\)00044-7](https://doi.org/10.1016/0167-2738(95)00044-7).
- [4] Y. Arachi, T. Asai, O. Yamamoto, Y. Takeda, N. Imanishi, K. Kawate, C. Tamakoshi, Electrical conductivity of ZrO_2 – Sc_2O_3 doped with HfO_2 , CeO_2 , and Ga_2O_3 , *J. Electrochem. Soc.* 148 (2001) A520–A523. <https://doi.org/10.1149/1.1366622>.
- [5] T.I. Politova, J.T.S. Irvine, Investigation of scandia–yttria–zirconia system as an electrolyte material for intermediate temperature fuel cells—influence of yttria content in system $(Y_2O_3)_x(Sc_2O_3)_{(11-x)}(ZrO_2)_{89}$, *Solid State Ionics* 168 (2004) 153–165. <https://doi.org/10.1016/j.ssi.2004.02.007>.
- [6] A. Spirin, V. Ivanov, A. Nikonov, et al., Scandia- stabilized zirconia doped with yttria: synthesis, properties, and ageing behavior, *Solid State Ionics* 225 (2012) 448–452. <https://doi.org/10.1016/j.ssi.2012.02.022>.
- [7] F.T. Ciacchi, S.P.S. Badwal, The system Y_2O_3 – Sc_2O_3 – ZrO_2 : phase stability and ionic conductivity studies, *J. Eur. Ceram. Soc.* 7 (1991) 197–206. [https://doi.org/10.1016/0955-2219\(91\)90037-Z](https://doi.org/10.1016/0955-2219(91)90037-Z).
- [8] V.V. Lakshmi, R. Bauri, Phase formation and ionic conductivity studies on ytterbia Co-doped scandia stabilized zirconia ($0.9ZrO_2$ – $0.09Sc_2O_3$ – $0.01Yb_2O_3$) electrolyte for SOFCs, *Solid State Sci.* 13 (2011) 1520–1525. <https://doi.org/10.1016/j.solidstatesciences.2011.05.014>.
- [9] V. Shukla, A. Kumar, I. Labbaveetil Basheer, K. Balani, A. Subramaniam, S. Omar, Structural characteristics and electrical conductivity of spark plasma sintered ytterbia Co-doped scandia stabilized zirconia, *J. Am. Ceram. Soc.* 100 (2017) 204–214. <https://doi.org/10.1111/jace.14545>.
- [10] F. Yuan, J. Wang, H. Miao, C. Guo, W.G. Wang, Investigation of the crystal structure and ionic conductivity in the ternary system $(Yb_2O_3)_x$ – $(Sc_2O_3)_{(0.11x)}$ – $(ZrO_2)_{0.89}$ ($x = 0$ – 0.11), *J. Alloys Compd.* 549 (2013) 200–205. <https://doi.org/10.1016/j.jallcom.2012.09.089>.
- [11] S. Omar, W.B. Najib, W. Chen, et al., Electrical conductivity of 10 mol% Sc_2O_3 –1 mol% M_2O_3 – ZrO_2 ceramics, *J. Am. Ceram. Soc.* 95 (2012) 1965–1972. <https://doi.org/10.1111/j.1551-2916.2012.05126.x>.
- [12] D.S. Lee, W.S. Kim, S.H. Choi, et al., Characterization of ZrO_2 Co-doped with Sc_2O_3 and CeO_2 , electrolyte for the application of intermediate temperature SOFCs, *Solid State Ionics* 176 (2005) 33–39. <https://doi.org/10.1016/j.ssi.2004.07.013>.
- [13] Z. Wang, M. Cheng, Z. Bi, Structure and impedance of ZrO_2 doped with Sc_2O_3 and CeO_2 , *Mater. Lett.* 59 (2005) 2579–2582. <https://doi.org/10.1016/j.matlet.2004.07.065>.
- [14] M. Liu, C. He, J. Wang, W.G. Wang, Z. Wang, Materials for intermediate temperature solid oxide fuel cell, *J. Alloys Compd.* 502 (2010) 319–323. <https://doi.org/10.1016/j.jallcom.2009.12.134>.
- [15] D.A. Agarkova, M.A. Borik, V.T. Bublik, S.I. Bredikhin, A.S. Chislov, A.V. Kulebyakin, I.E. Kuritsyna, E.E. Lomonova, F.O. Milovich, V.A. Myzina, V.V. Osiko, N.Yu. Tabachkova, Structure and transport properties of melt grown Sc_2O_3 and CeO_2 doped ZrO_2 crystals, *Solid State Ionics* 322 (2018) 24–29. <https://doi.org/10.1016/j.ssi.2018.04.024>.
- [16] M.A. Borik, S.I. Bredikhin, V.T. Bublik, A.V. Kulebyakin, I.E. Kuritsyna, E.E. Lomonova, F.O. Milovich, V.A. Myzina, V.V. Osiko, P.A. Ryabochkina, N.Y. Tabachkova, Structure and conductivity of yttria and scandia doped zirconia crystals grown by skull melting, *J. Am. Ceram. Soc.* 100 (2017) 5536–5547. <https://doi.org/10.1111/jace.15074>.
- [17] S. Omar, N. Bonanos, Ionic conductivity ageing behaviour of 10 mol.% Sc_2O_3 –1 mol.% CeO_2 – ZrO_2 ceramics, *J. Mater. Sci.* 45 (2010) 6406–6410. <https://doi.org/10.1007/s10853-010-4723-x>.
- [18] C.N.S. Kumar, R. Bauri, Enhancing the phase stability and ionic conductivity of scandia stabilized zirconia by rare earth co-doping, *J. Phys. Chem. Solids* 75 (2014) 642–650. <https://doi.org/10.1016/j.jpcs.2014.01.014>.
- [19] J. Kondoh, S. Kikuchi, Y. Tomii, Y. Ito, Effect of aging on yttria-stabilized zirconia: I. A study of its electrochemical properties, *J. Electrochem. Soc.* 145 (1998) 1527–1536. <https://doi.org/10.1149/1.1838515>.
- [20] J. Kondoh, S. Kikuchi, Y. Tomii, Y. Ito, Effect of aging on yttria-stabilized zirconia: II. A study of the effect of the microstructure on conductivity, *J. Electrochem. Soc.* 145 (1998) 1536–1550. <https://doi.org/10.1149/1.1838516>.
- [21] B. Butz, P. Krus, H. Störmer, D. Gerthsen, A. Müller, A. Weber, E. Ivers-Tiffée, Correlation between microstructure and degradation in conductivity for cubic Y_2O_3 -doped ZrO_2 , *Solid State Ionics* 177 (2006) 3275–3284. <https://doi.org/10.1016/j.ssi.2006.09.003>.
- [22] M.A. Borik, S.I. Bredikhin, V.T. Bublik, A.V. Kulebyakin, I.E. Kuritsyna, E.E. Lomonova, N.Y. Tabachkova, The impact of structural changes in ZrO_2 – Y_2O_3 solid solution crystals grown by directional crystallization of the melt on their transport characteristics, *Mater. Lett.* 205 (2017) 186–189. <https://doi.org/10.1016/j.matlet.2017.06.059>.
- [23] V.V. Osiko, M.A. Borik, E.E. Lomonova, Synthesis of refractory materials by skull melting, in: G. Dhanaraj, K. Byrappa, V. Prasad, M. Dudley (Eds.), *Springer Handbook of Crystal Growth*, Springer, New York, 2010, pp. 433–477.
- [24] T. Sakuma, H. Suto, The cubic-to- β martensitic transformation in ZrO_2 – Sc_2O_3 , *J. Mater. Sci.* 21 (1986) 4359–4365. <https://doi.org/10.1007/BF01106556>.
- [25] Y. Hemberger, N. Wichtner, C. Berthold, K.G. Nickel, Quantification of Yttria instabilized zirconia by Raman spectroscopy, *Int. J. Appl. Ceram. Technol.* 13 (2016) 116–124. <https://doi.org/10.1111/ijac.12434>.
- [26] M. Yashima, S. Sasaki, M. Kakihana, Y. Yamaguchi, H. Arashi, M. Yoshimura, Oxygen-induced structural-change of the tetragonal phase around the tetragonal-cubic phase-boundary in ZrO_2 – $YO_{1.5}$ solid-solutions, *Acta Crystallogr. B* 50 (1994) 663–672. <https://doi.org/10.1107/S0108768194006257>.
- [27] W. Araki, T. Koshikawa, A. Yamaji, T. Adachi, Degradation mechanism of scandia-stabilised zirconia electrolytes: discussion based on annealing effects on mechanical strength, ionic conductivity, and Raman spectrum, *Solid State Ionics* 180 (2009) 1484–1489. <https://doi.org/10.1016/j.ssi.2009.09.001>.